# Prolonged oscillating kisspeptin neuron activity underlies the preovulatory luteinizing hormone surge in mice

Ziyue Zhou, Cheng-Yu Huang and Allan E. Herbison

Department of Physiology, Development and Neuroscience, University of Cambridge, Cambridge CB2 3EG, UK

**Corresponding author:** Allan E. Herbison aeh36@cam.ac.uk

**Disclosures:** The authors have nothing to disclose and no competing interests.

**Abstract**

The population of kisspeptin neurons located in the rostral periventricular area of the third ventricle (RP3V) is thought to have a key role in generating the GnRH surge that triggers ovulation. Using a modified GCaMP fibre photometry procedure, we have been able to record the in vivo population activity of RP3V$^{KISS}$ neurons across the estrous cycle of female mice. A marked increase in GCaMP activity was detected beginning on the afternoon of proestrus that lasted in total for 13±1 hours. This was comprised of slow baseline oscillations with a period of 91±4 min and associated with high frequency rapid transients. Very little oscillating baseline or transient activity was detected at other stages of the estrous cycle. Concurrent blood sampling showed that the peak of the LH surge occurred 3.5±1.1 h after the first baseline RP3V$^{KISS}$ neuron baseline oscillation on the afternoon of proestrus. The time of onset of RP3V$^{KISS}$ neuron oscillations varied between mice and across subsequent proestrous stages in the same mice. To assess the impact of estradiol on RP3V$^{KISS}$ neuron activity, mice were ovariectomized and given an incremental estradiol replacement regimen. Minimal patterned GCaMP activity was found in OVX mice, and this was not changed acutely by any of the estradiol treatments. However, on the afternoon of the expected LH surge, the same oscillating baseline activity with associated transients occurred for 7.1±0.5 h. These observations reveal an unexpected prolonged oscillatory pattern of RP3V$^{KISS}$ neuron activity that is dependent on estrogen and underlies the preovulatory LH surge as well as potentially other facets of reproductive behavior.

## Introduction

A neural surge generator is responsible for integrating multiple signals to control the mid-cycle activation of GnRH neurons that triggers the preovulatory luteinizing hormone (LH) surge (Herbison 2015, Kauffman 2022). It now seems clear that a preoptic area population of kisspeptin neurons that directly activate GnRH neuron cell bodies (Piet, Kalil et al. 2018) is an essential component of the surge generator in spontaneously ovulating mammals (Matsuda, Ohkura et al. 2019, Goodman, Herbison et al. 2022).

The primary regulator of surge generator activity in spontaneously ovulating species is the gradually increasing levels of circulating estradiol that occur throughout the follicular phase of the cycle. In rodents, this "estrogen positive feedback" mechanism is mediated by estrogen receptor alpha (ESR1) and occurs within the rostral periventricular area of the third ventricle (RP3V) (Wintermantel, Campbell et al. 2006, Porteous and Herbison 2019); a preoptic brain region encompassing the anteroventral periventricular nucleus (AVPV) and periventricular preoptic nucleus (PeN) (Herbison 2008). In vivo CRISPR/Cas9 gene editing to knockdown ESR1 expression selectively in RP3V kisspeptin ($RP3V^{KISS}$) neurons has been shown to suppress both the LH surge and estrous cyclicity in adult female mice (Wang, Vanacker et al. 2019, Clarkson, Yip et al. 2023). Although of variable importance amongst mammalian species, a circadian input to the surge generator is also critical for the GnRH surge in rodents (Goodman, Herbison et al. 2022). It remains unclear how this operates, but a vasopressin input from the suprachiasmatic nucleus to the $RP3V^{KISS}$ neurons is suspected to be important in triggering the onset of the surge (Tonsfeldt, Mellon et al. 2022, Piet 2023).

The ability to monitor the activity of arcuate nucleus (ARN) kisspeptin neurons in freely behaving mice with GCaMP fibre photometry has been invaluable in defining and then understanding their role as the GnRH pulse generator in puberty and adulthood, as well as in pathological states (Clarkson, Han et al. 2017, Han, Kane et al. 2019, McQuillan, Han et al. 2019, Liu, Yeo et al. 2021, McQuillan, Clarkson et al. 2022, Goto, Hagihara et al. 2023, Han, Morris et al. 2023, Goto, Hagihara et al. 2025, Zhou, Han et al. 2025). To date, attempts to record the behaviour of the $RP3V^{KISS}$ neurons have been unsuccessful due primarily to the vertical column-like topography of the $RP3V^{KISS}$ neurons alongside the third ventricle. Indeed, attempts by us to employ bevelled or mirror lenses that gather fluorescence from the side of the optic fibre have been met with very limited success. We now report here the use of tapered optic fibres (Pisano, Pisanello et al. 2019) that enable the population activity of $RP3V^{KISS}$ neurons to be monitored in real time in freely behaving mice. This reveals the estrogen-dependent dynamics of $RP3V^{KISS}$ neuron population activity across the estrous cycle and reveals an unexpected oscillatory pattern of synchronised activity that continues for over 12 hours on proestrus.

## Results

### *Characterization of GCaMP expression in RP3V$^{KISS}$ neurons*

Adult *Kiss1$^{Cre/+}$* (Palmiter v2) female mice (Padilla, Johnson et al. 2018) were injected bilaterally with recombinant Cre-dependent AAVs encoding GCaMP6s. As the relationship of Cre-driven expression to kisspeptin immunoreactivity has not been reported for the RP3V in this line, we undertook dual label immunofluorescence for GFP (GCaMP6s) and kisspeptin in 5 female mice killed on proestrus. All mice exhibited many GFP-immunoreactive cells (33.0 ± 5.9 cells/section) located primarily adjacent to the third ventricle within the preoptic area (Fig.1A) and this exhibited overlap with kisspeptin immunoreactivity (21.8 ± 3.1 cells/section) (Fig.1B&C). However, the numbers of clearly identifiable dual labelled cells were 10.4 ± 2.5/section resulting in 47.0 ± 5.7% of kisspeptin-immunoreactive neurons expressing GCaMP6s and 33.0 ± 5.5% of GFP cells expressing clearly cytoplasmic kisspeptin immunoreactivity. These relatively low levels of Cre-targeted expression, compared to ARN kisspeptin neurons, are typical for RP3V kisspeptin neurons in other Kiss1-Cre lines (Yip, Boehm et al. 2015, Yeo, Kyle et al. 2016, Piet, Kalil et al. 2018). This presumably results from the difficulty of detecting kisspeptin immunoreactivity in the cytoplasm of all RP3V kisspeptin neurons. *Kiss1-Cre* negative proestrus female mice given AAV injections (N=2) did not exhibit any GFP/GCaMP6s expression.

### *RP3V$^{KISS}$ neuron population activity across the estrous cycle*

To make fibre photometry recordings from RP3V kisspeptin neurons, mice were given unilateral injections of AAV9-CAG.FLEX.GCaMP6s into the RP3V of adult *Kiss1$^{Cre/+}$* female mice followed by the implantation of a tapered optic fibre (Fig.2A). Three weeks later, mice were recorded continuously across each day of the estrous cycle. The GCaMP signals recorded from RP3V$^{KISS}$ neurons (N=8) showed minimal fluctuations during metestrus and diestrus but became markedly more active on the afternoon of proestrus displaying an oscillatory pattern of increased baseline fluorescence associated with high frequency transients (Fig.2B,C). This heightened activity gradually subsided by the morning of estrus before returning to a quiescent state (Fig.B,C). An assessment of relative activity across the estrous cycle using area under the curve (AUC) demonstrated a significant increase in GCaMP fluorescence on proestrus compared to all of the other stages (Friedman Test: $\chi^2$=16.2, p=0.0010; Dunn's multiple comparisons tests: p=0.0402 (metestrus), p=0.006 (diestrus), p=0.0402 (estrus); Fig.2D). Two mice with misplaced optic fibres exhibited almost no baseline activity (Fig.2E,F).

### *RP3V$^{KISS}$ neuron population activity in relation to the LH surge on proestrus*

To examine the relationship between the increased activity of RP3V$^{KISS}$ neurons and the LH surge on proestrus, tail-tip bleeding was undertaken at 2–4-hour intervals for 8-10 hours (N=5). Peak LH levels (18.0 ± 3.2 ng/ml) occurred 3.5 ± 0.4 hours after the first RP3V$^{KISS}$ neuron oscillation was detected with oscillations then continuing for a further 7.4 ± 1.6 hours after the decline in LH levels (Fig.3A,B).

### *Oscillating baseline shifts in RP3V$^{KISS}$ neuron population activity on proestrus*

To provide a detailed analysis of the GCaMP signals recorded on proestrus, a customised MATLAB code was used to separate slow and fast signal components. A 30-minute moving average was applied to the original dF/F signal (Fig.3C,D i) to extract the slow baseline changes in GCaMP

activity (Fig.3C,D ii). Subtraction of this baseline from the original signal leaves the high frequency transients (Fig.3C,D iii).

The baseline shifts in GCaMP fluorescence exhibited a consistent oscillatory pattern on proestrus in all 8 mice (Fig.3C,D ii & Fig.4C). The first identified oscillation was observed to begin 3.7 ± 0.5 hours (range: 1.6-5.3 hours) before lights-off with the total duration of oscillatory behaviour lasting 12.7 ± 0.7 hours (range: 10.0-15.0 hours) (Fig.4C,E). The mean duration of each slow oscillation was 90.8 ± 4.4 minutes (range: 39.3-166.1 minutes). Oscillations were occasionally observed in other stages of the cycle (3 of the 8 mice) and these had similar durations (metestrus: 88.6 ± 9.5 minutes, diestrus: 120.4 ± 29.7 minutes, estrus: 91.9 ± 21.7 minutes; Kruskal-Wallis test: $\chi^2$=1.65, p=0.65). The numbers of oscillations observed on proestrus were substantially greater than at all other stages of the cycle (Friedman Test: $\chi^2$=18.75, p=0.0003; Dunn's multiple comparisons tests: p=0.0402 (metestrus), p=0.0029 (diestrus), p=0.0117 (estrus); Fig.4E) and had significantly higher amplitudes (Friedman Test: $\chi^2$=17.86, p=0.0005; Dunn's multiple comparisons tests: proestrus 7.2 ±0.9; metestrus 1.9 ± 1.0 p=0.0221, diestrus 1.1 ± 0.8 p=0.0084, estrus 1.5 ± 0.8 p=0.0084). Interestingly, a consistent ~90-minute oscillation started one hour preceding "lights-off" throughout the estrous cycle (Fig.4F).

### *High frequency transient activity in RP3V$^{KISS}$ neuron population activity*

After baseline correction, high frequency transients were identified using a z-scoring approach, where dF/F traces were normalised and thresholded across multiple values (k = 1 to 4, step 0.2). This method provides a data-driven, threshold-independent way to detect transients while reducing the impact of noise and ensuring robustness across different signal amplitudes.

Transient activity was detected throughout the estrous cycle but had its highest frequency on proestrus (Repeated measures one-way ANOVA: F=24,35, p<0.0001; Tukey's multiple comparisons tests: p=0.0025 (metestrus), p=0.0003 (diestrus), p=0.0008 (estrus); Fig.5A,B). Similarly, the amplitude of individual transients was higher in proestrus compared to other stages (Repeated measures one-way ANOVA: F=35.58, p=0.0001; Tukey's multiple comparisons tests: p=0.0032 (metestrus), p=0.0010 (diestrus), p=0.0014 (estrus); Fig.5A,C). Each transient typically had a duration of ~10 s and this changed slightly across the cycle being longer in proestrus compared to estrus (Repeated measures one-way ANOVA: F=7.71, p=0.0059; Tukey's multiple comparisons tests: p=0.0053), with transients also being longer in metestrus when compared to diestrus (Tukey's multiple comparisons tests: p=0.040) (Fig.5D). When aligning high frequency transients with baseline oscillations, the up-state of each oscillation appears to coincide with an increased frequency of transients, whereas the troughs in the baseline correlate with a slower frequency of transients (Fig.3C,D iv).

### *Shifting onset of RP3V$^{KISS}$ neuron population activation across subsequent proestrous stages*

The onset of GnRH neuron surge activity exhibits substantial variability between mice and also within cycles in individual mice (Han, Yeo et al. 2025). To examine the consistency of the surge-like behaviour observed in proestrus, RP3V$^{KISS}$ neuron activity was recorded across two or three

proestrous stages in the same mouse and GCaMP signals were deconvolved to assess baseline shifts.

All seven mice exhibited variability in the initiation and duration of oscillatory activity occurring during proestrus across different cycles (Fig.6A,B). On average, the peak of the first oscillation varied by 2.0 ± 0.5 hours when examining surge activity in the same mice (range: 0.4-4.2 hours; n=7). There was no consistent pattern in surge onset timing across subsequent proestrous surges with mice fluctuating both forward and backward (Fig.6A,B).

### *RP3V$^{KISS}$ neuron population activity in OVX, estrogen-replaced female mice*

Rising follicular phase levels of estradiol (E2) are the key signal driving the GnRH surge generator. To examine the effect of estradiol on RP3V$^{KISS}$ neuron activity, five of the mice reported above were ovariectomised (OVX) and subjected to a well-established estrogen replacement regimen involving the placement of E2-containing Silastic capsules followed by s.c. injection of estradiol benzoate (EB) (Bronson 1981) (Fig.7). This also provided within-animal comparisons between intact and OVX states as well as the proestrous and OVX+E2+EB-induced surges.

Mice examined one week after OVX exhibited a significant decrease in RP3V$^{KISS}$ neuron population activity compared with the intact (diestrus) state (Figs.7A,B & 8A; Paired t-test: p=0.002). Despite an upward trend, the subsequent replacement of E2 did not result in any significant change in RP3V$^{KISS}$ neuron activity 5 days after capsule implantation (Figs.7B,C & 8B) (Friedman test: $\chi^2$=10.68, p=0.0055 for all groups; Dunn's multiple comparisons tests: p=0.26 (OVX vs OVX+E2)). This procedure has been shown previously to return estradiol to physiological diestrus levels (Porteous, Haden et al. 2021). Similarly, the injection of EB on day 6 did not have any significant effect on GCaMP signal in OVX+E2+EB mice (Fig.7C,D & 8B) Dunn's multiple comparisons tests: p>0.99 (OVX vs OVX+E2+EB). However, the following day, when an LH surge was expected, RP3V$^{KISS}$ neuron activity became elevated with the appearance of baseline oscillations and enhanced transient activity (Fig.7E) with a significant increase in AUC fluorescence compared with OVX mice (Dunn's multiple comparisons tests: p=0.021; Fig.8B). Qualitatively, the pattern of RP3V$^{KISS}$ neuron surge activity appeared similar on proestrus and OVX+E2+EB in the same mice (FIG.7E,F) but the magnitude of change was substantially reduced in the OVX+E2+EB condition (paired t-test: p=0.014; Fig.8C).

To evaluate RP3V$^{KISS}$ neuron activity in more detail in the OVX+E2+EB paradigm, the same deconvolution methods employed for the intact recordings were used (Fig.8D,E). Three of five females exhibited identified oscillations in OVX+E2+EB surge state with 3.7 ± 0.3 oscillations (range: 3-4 oscillations) occurring during the recording period and these had a duration of 88.6 ± 10.1 minutes per oscillation (range: 59.7-169.3 minutes), and an amplitude of 4.5 ± 1.2% (range: 2.2-6.1%). Average total duration of oscillatory activity in these mice was 7.1 ± 0.5 hours (range: 6.1-8.0 hours); significantly shorter compared to that of proestrus (unpaired t-test, p=0.001). During the other treatment conditions, only one out of five females exhibited a single identified oscillation on the day of EB injection (OVX+E2+EB).

Notably, the oscillation observed ~1h before lights-off in intact mice disappeared after OVX but appeared to be restored under all estrogen replacement conditions (Fig.8D).

The high frequency transients (Fig.8E) were evaluated across all four conditions. The frequency of transients was significantly elevated during the OVX+E2+EB surge condition compared to OVX (Friedman test: $\chi^2$=14.04, p<0.0001; Dunn's multiple comparisons tests: p=0.0014) (Fig.8E, Table 1). The durations of transients were not different across conditions (Table 1., Repeated measures one-way ANOVA: F=0.50, p=0.53). Although repeated measures one-way ANOVA revealed a significant main effect of estrogen treatment on transient amplitude (F=8.1, p=0.039), post-hoc analysis using Tukey's multiple comparisons tests did not detect any significant pairwise differences between individual conditions (Table 1).

Table 1: High frequency transients parameters in different treatment groups (Mean ± SEM)

| Treatment | Frequency (Hz) | Duration (seconds) | Amplitude (dF/F %) |
|---|---|---|---|
| OVX | 0.0020 ± 0.00046 | 14.36 ± 1.85 | 2.30 ± 0.22 |
| OVX+E2 | 0.0038 ± 0.00028 | 14.34 ± 0.86 | 2.47 ± 0.26 |
| OVX+E2+EB | 0.0044 ± 0.00029 | 13.40 ± 0.79 | 2.55 ± 0.27 |
| OVX+E2+EB surge | 0.0120 ± 0.00190 | 13.13 ± 1.00 | 3.03 ± 0.39 |

**Discussion**

We report here that RP3V$^{KISS}$ neurons exhibit a marked increase in population activity on the afternoon of proestrus consisting of 90-min duration oscillations associated with high frequency transient activity that last for approximately 13 hours. Given prior evidence (Goodman, Herbison et al. 2022, Kauffman 2022), the first half of this activation period almost certainly drives the proestrous LH surge while the role of the latter activity remains less certain. We show that this behavior of RP3V$^{KISS}$ neurons is driven by circulating estradiol although the standard OVX+E2+EB model of estrogen replacement used here appears insufficient to drive the normal magnitude of RP3V$^{KISS}$ neuron activity.

The activity of the RP3V$^{KISS}$ neuron population is relatively stable during metestrus and diestrus with only very occasional excursions from basal activity. This changes markedly on the afternoon of proestrus when substantial baseline oscillations associated with large amounts of transient activity are recorded for the next ~ 13 hours. It appears as though the onset of this activity occurs well before the start of the LH surge as the peak of the surge occurred 3-4 hours after the onset of oscillatory RP3V$^{KISS}$ neuron activity. While the temporal resolution of our blood sampling (hours) is poor compared to that of the neural recordings (seconds), elevated oscillatory RP3V$^{KISS}$ neuron activity was always present at 13:00 h when LH levels were low in the 5 mice examined. In contrast, GnRH neuron activity on proestrus is much more coincident with the onset of the LH surge (Han, Yeo et al. 2025). This suggests that despite the potent and abrupt activation of GnRH neurons by exogenous kisspeptin (Han, Gottsch et al. 2005) or by optogenetic activation of RP3V$^{KISS}$ neurons (Piet, Kalil et al. 2018), a sustained period of rising RP3V$^{KISS}$ neuron activity may normally occur to activate the GnRH neurons to induce the surge.

We also find that RP3V$^{KISS}$ neuron activity continues for many hours past the peak of the LH surge. This is the same as the profile of GnRH neuron activity in the mouse on proestrus (Han, Yeo et al. 2025, Liu, Shen et al. 2025)(Fig.9) and long-standing observation that GnRH secretion at the median eminence long outlasts the LH surge in multiple species (Sarkar, Chiappa et al. 1976, Pau, Berria et al. 1993, Karsch, Bowen et al. 1997). While it remains unclear what the role of GnRH secretion after the LH surge may be (Skinner and Caraty 2002), it is very likely that the extended period of GnRH and LH secretion is driven by prolonged RP3V$^{KISS}$ neuron input to the GnRH neurons.

The impact of extended proestrus RP3V$^{KISS}$ neuron activity on other neural networks in the forebrain remain unknown. The RP3V$^{KISS}$ neurons project widely throughout the limbic forebrain (Yeo and Herbison 2011) and may conceivably operate to coordinate multiple functions relevant to reproduction at proestrus. Indeed, commensurate with the long period of elevated RP3V$^{KISS}$ neuron activity detected here following the surge, these neurons have been proposed to have a role in modulating female mate preference and copulatory behavior (Hellier, Brock et al. 2018) that would typically occur a few hours after the surge. At present, a detailed analysis of RP3V$^{KISS}$ neurons projections is lacking and it remains unknown whether the sub-population of RP3V$^{KISS}$ neurons innervating GnRH neurons also send collaterals to other brain regions.

The recent ability to record the activity of the GnRH neuron population in vivo revealed that their elevated activity on the afternoon of proestrus occurred in an oscillatory manner with a period of ~ 78 min (Han, Yeo et al. 2025). This provides a striking parallel with the ~ 91 min-duration oscillations now detected in RP3V$^{KISS}$ neurons activity over the exact same time period. This suggests that the unusual oscillatory pattern of GnRH neuron activity on proestrus is being driven by RP3V$^{KISS}$ neurons. Indeed, the entire profile of RP3V$^{KISS}$ and GnRH neuron activity across proestrus is strikingly similar (Fig.9) making it very likely that GnRH neuron activity on proestrus is patterned almost entirely by the RP3V$^{KISS}$ neurons. Nevertheless, a small role may also exist for the ARN kisspeptin neuron pulse generator as it remains active during the ascending phase of the proestrous LH surge (McQuillan, Han et al. 2019, Han, Yeo et al. 2025). As such, the episodic release of kisspeptin from the ARN pulse generator on GnRH neuron dendrons may potentiate early GnRH secretion driven by RP3V$^{KISS}$ neurons. However, the functional impact of ARN kisspeptin neurons on the surge remains unclear in mice as the deletion of ARN kisspeptin neurons was not found to have any effect on the LH surge (Coutinho, Esparza et al. 2024) while selective removal of kisspeptin from ARN neurons resulted in a decrease in the amplitude of the LH surge (Velasco, Franssen et al. 2023).

It is interesting to speculate on how oscillatory activity may be generated in RP3V$^{KISS}$ neurons and what role it may play. We find that the baseline GCaMP oscillations are associated with intense high frequency transient activity with each transient having a duration of approximately 10 s. This may represent the signature of single or small groups of RP3V$^{KISS}$ neurons exhibiting 10 s burst firing that then go on to synchronise into 90 min episodes of activity. In acute brain slices, RP3V$^{KISS}$ neurons often exhibit spontaneous burst firing (Jamieson and Piet 2022) and each burst is known to generate 5-10 s-duration calcium transients in GCaMP recordings (Piet, Fraissenon et al. 2015). It is also interesting to note that the optogenetic induction of burst firing in RP3V$^{KISS}$ neurons is the most efficient mode for activating GnRH neurons and LH secretion (Piet, Kalil et al. 2018). How RP3V$^{KISS}$ neurons may synchronise their activity is unknown. It is possible that, like ARN kisspeptin

neurons, they use direct recurrent collateral innervation to facilitate periods of synchronous bursting. Alternatively, synchronicity may be generated within a wider network of RP3V circuitry and/or by afferent inputs. The physiological roles and necessity for episodic activity in GnRH neurons, driven by RP3V$^{KISS}$ neurons, are also unknown. As these neurons are required to be intensely active for prolonged periods of over 12 hours, it is possible that recurrent episodes of inhibition protect RP3V$^{KISS}$ and GnRH neurons from excitotoxicity.

It is well established that the onset of the LH surge is entrained by circadian inputs in rodents (Tonsfeldt, Mellon et al. 2022, Piet 2023). However, this entrainment is not highly time locked compared to other circadian-timed events such as locomotion (Starnes and Jones 2023). We show here that the onset of RP3V$^{KISS}$ neuron activity between mice, and even within the same mouse, varies by several hours around the time of "lights off" on proestrus. The exact same observations have been made for GnRH neuron activation and the LH surge on proestrus (Miller, Olson et al. 2004, Minabe, Uenoyama et al. 2011, Czieselsky, Prescott et al. 2016, Yeo, Han et al. 2025). Given this variability, we were surprised to observe a tightly time-locked RP3V$^{KISS}$ neuron increment in activity almost exactly one hour before "lights off" on proestrus, as well as on every other day of the cycle. While this would appear to be a rigid circadian input to the RP3V$^{KISS}$ neurons, its role in triggering the LH surge is unclear and will require further investigation. Interestingly, OVX mice were the only group in which we did not observe this circadian event. This dependence on estrogen is reminiscent of the excitatory effect of vasopressin on RP3V$^{KISS}$ neuron firing that is unchanging in different estrogenic states but absent in OVX mice (Piet, Fraissenon et al. 2015).

We find that the activity of the RP3V$^{KISS}$ neuron population is reduced 7-days following ovariectomy but that relatively little change is evoked by a sequential regimen of estrogen replacement until the day of the expected surge when proestrus-like oscillatory activity emerges. This is consistent with the concept of the surge being generated by rising estrogen levels that harness slow transcriptional mechanisms to alter RP3V$^{KISS}$ neuron excitability (Glidewell-Kenney, Hurley et al. 2007, Herbison 2015). Increments in circulating estradiol either in the OVX+E model or during diestrus, when estradiol levels peak (Wall, Desai et al. 2023), appear to have little immediate effect on RP3V$^{KISS}$ neuron activity patterns. This is broadly in agreement with acute brain slice studies that have consistently found reduced RP3V$^{KISS}$ neurons firing rates following OVX but then rather few consistent changes in firing across the estrous cycle itself (Jamieson and Piet 2022). Nevertheless, it is clear that estrogen treatment of OVX mice slowly up-regulates sodium ($I_{NaP}$), calcium ($I_T$), and hyperpolarization-activated ($I_h$) ion channels in RP3V$^{KISS}$ neurons, that would all be expected to result in increased excitability (Jamieson and Piet 2022). Once established, these changes in ion channel expression are presumably at least partly responsible for the enhanced oscillatory-like activity patterns of RP3V$^{KISS}$ neurons observed on the day of the surge.

While the same pattern of RP3V$^{KISS}$ neuron activity is observed on the afternoon of proestrus and in the OVX+E2+EB model, it is evident that the magnitude of change is dramatically reduced in the latter. Although we did not assess surge LH levels in the OVX+E2+EB mice used in this study, prior work from the laboratory using the same model has shown that peak LH surge levels (7.7±0.7 ng/mL) are half of that observed on proestrus (14.5±1.5 ng/mL) (Czieselsky, Prescott et al. 2016). This inability to recreate proestrous-like LH surge levels is typical in estrogen-replaced OVX mouse models (Bronson and Vom Saal 1979, Dror, Franks et al. 2013, Silveira, Burger et al. 2017). We

would suggest that the reduced amplitude of the LH surge in estrogen-replaced OVX models likely originates from sub-optimal activation of the RP3V$^{KISS}$ neurons. This may be due to the lack of progesterone or other ovarian factors in estrogen-replaced OVX models. However, it is important to note that the seminal experiments of Bronson and Vom Saal (Bronson and Vom Saal 1979) identified that a full LH surge can be achieved in OVX+E2+EB mice with careful attention to the timing of the EB injection. Our present OVX+E2+EB protocol matches the most efficacious protocol of Bronson and Vom Saal with the exception of using 4 compared to 5 µg E2 capsules and a 12:12 rather than 14:10 lighting regimen.

In summary, we demonstrate that RP3V$^{KISS}$ neurons exhibit an unusual, extended period of baseline oscillatory activity on proestrus. The genesis of oscillatory RP3V$^{KISS}$ neuronal activity is critically dependent on long-term exposure to estradiol with a less clear involvement of circadian inputs. This oscillatory RP3V$^{KISS}$ neuron activity almost certainly drives the same pattern of GnRH neuron activity detected at this time which is critical for triggering the preovulatory LH surge. It possible that the oscillatory RP3V$^{KISS}$ neuron activity existing beyond the generation of the LH surge operates to coordinate other neural circuits controlling reproduction such as those underlying female sexual behavior (Hellier, Brock et al. 2018).

## Materials and Methods

*Animals*

Adult *B6(129S4)-Kiss1*$^{tm1.1(cre/EGFP)Rpa}$*/J* (Palmiter *Kiss1*$^{Cre/+}$ (v2), JAX stock #033169) (Padilla, Johnson et al. 2018) female mice were group-housed in conventional cages with environmental enrichment under conditions of controlled temperature (22±2$^{0}$C) and lighting (12-hour light/12-hour dark cycle; lights on at 07:00) with *ad libitum* access to water and low-phytoestrogen food (Tekland 2016, Envigo RMS, UK) and water. Following surgery, mice were single housed in conventional cages under the same conditions until the end of the study. All animal experimental protocols were approved by the University of Cambridge Animal Welfare and Ethics Review Body under UK Home Office licenses P174441DE and PP9818192.

*Stereotaxic implantation of optic fibres and AAV injections*

Adult female mice (10-14-weeks-old) were anaesthetised with 2% isoflurane and placed in a stereotaxic frame with buprenorphine (0.05mg/kg, s.c.) and meloxicam (5 mg/kg, s.c.) analgesia. Dexamethasone (10 mg/kg, s.c.) was used to prevent cranial swelling. A custom-built Hamilton syringe apparatus, holding a 5-µL Hamilton syringe (Hamilton, catalogue No. 7634-01) with a 29-gauge bevelled needle (Hamilton, catalogue No. 90029), was filled with 2.0 µL of recombinant Cre-dependent AAVs encoding GCaMP6s (AAV9CAG.FLEX.GCaMP6s.WPRE.SV40, Addgene, Catalogue, No. AG0334, titre: 2 x $10^{13}$ genome copy/mL). Mice for photometry experiments received a single unilateral injection of 2.0 µL AAV at coordinates 0.8 mm anterior to bregma, 0.25 mm lateral to the superior sagittal sinus, and 5.0 mm deep. Mice for immunohistochemistry characterisation received bilateral AAV injections. After a unilateral viral injection, an indwelling

tapered optical fibre (400 µm diameter, 0.66 NA, 3.5 mm taper length, Doric Lenses, Quebec, Canada) was implanted directly into the RP3V on the same side (0.55 mm anterior to bregma, 0.22 mm lateral to the superior sagittal sinus, 5.2 mm deep). One week following surgery, all animals were handled daily and habituated to a photometry recording set-up for at least three weeks. Estrous cycle stage was assessed by vaginal lavage each morning.

*Estrogen-induced surge model*

All estrogen-induced surge studies in the laboratory use the OVX+E2+EB protocol of Bronson and Vom Saal with slight modifications (Bronson and Vom Saal 1979). One week after OVX, mice were implanted subcutaneously with silastic implants (id, 1.02 mm; od, 2.16 mm, Dow Corning Corp) containing 4 µg 17β-estradiol (E2, Sigma-Aldrich, catalogue No. E8875) per 20 g body weight. This dose of 4 µg has been shown to return E2 levels to diestrous concentrations (Porteous, Haden et al. 2021). Six days after capsule implantation, mice were given a subcutaneous injection of 1 µg β-estradiol 3-benzoate (EB, Sigma-Aldrich, catalogue No. E8875) in 100 µL sesame oil at 09:00 hours, two hours after lights on. This protocol evokes an LH surge the following day (Fig.7).

To assess the relationship between $RP3V^{KISS}$ neuron and the proestrous LH surge, female mice were attached to the fibre photometry system in the morning of proestrus and tail-tip blood samples (5-µL) collected every 2-4 hours over a period of 8-10 hours (Czieselsky, Prescott et al. 2016). Levels of LH were measured by LH ELISA (Kreisman, McCosh et al. 2022) with a sensitivity of 0.07 ng/mL and intraassay and interassay coefficients of variation of 8.2% and 11.1%, respectively.

*Immunohistochemistry*

Female mice receiving bilateral injections of Cre-dependent AAVs encoding GCaMP6s were perfused with ice-cold 4% paraformaldehyde (PFA) on the afternoon of proestrus at least three weeks after viral injections. Brains were removed and post-fixed in 4% PFA for 4 hours before transferred to 30% sucrose. Forty-µm-thick coronal sections were cut on a freezing microtome for immunofluorescence. Brain sections were incubated with polyclonal rabbit anti-kisspeptin antisera, raised against the final ten amino acids of murine kisspeptin (1:5,000; AC566, Dr. Alain Caraty, Nouzilly, France) and chicken anti-GFP (1:5,000 Aves Lab, catalogue No. GFP-1020) for 72 hours. Brain sections were the washed and incubated with biotinylated goat anti-rabbit IgG (1:500; Vector Laboratories, catalogue No. BA-1000) followed by Streptavidin Alexa Fluor 568 (1:500; Invitrogen, Thermofisher, catalogue No. S11226) and goat anti-chicken Alexa Fluor 488 (1:1,000; Molecular Probes, Thermofisher, catalogue No. A-11039).

Immunofluorescent images were taken on a laser scanning confocal microscope (Zeiss LSM900) using a 20x objective lens in z-stacks with 2 µm steps across the depth of the slide. The numbers of GFP-expressing, kisspeptin-expressing, and co-expressing cell bodies were manually counted using ImageJ.

*GCaMP6 fibre photometry and blood sampling*

GCaMP6 fibre photometry was set up as previously described (Clarkson, Han et al. 2017). Fluorescence signals were sampled at 10 Hz using a scheduled mode (2 seconds on/ 2 seconds

off) of light emission with custom software (Tussock Innovation). Twenty two-hour recordings were made from mice across each stage of the estrous cycle, 1 week after ovariectomy, and during different times of the OVX+E2+EB surge protocol (Fig.7); with all starting 4 hours after lights-on.

Analysis of fluorescent signals was performed in MATLAB with the subtraction of the 405 signal from the 465 signal to extract the calcium-dependent fluorescence signal. Fluorescent signals were then down-sampled by averaging each 2-second recording during the 4-second on-off period into a single data point. An exponential fit algorithm was used to correct for baseline shifts using a 6-hour window before the signal was calculated in dF/F (%) with the equation $dF/F = (F_{fluorescence}-F_{baseline})/ F_{baseline}) \times 100$.

Numpy.trapezoid function was used in Python to calculate the definite integral of the curve, approximating the area under the curve (AUC) using the trapezoidal rule. Deconvolution of signals was achieved by applying the movmean algorithm in MATLAB to extract a 30-minute rolling average (Han, Yeo et al. 2025). With this approach, slow oscillations in baseline were then identified by findpeaks function in MATLAB with a) a minimum peak height set as two standard deviations above the mean calcium signal from 11:00-13:00 hours, b) minimum peak distance as 30 minutes, and c) minimum peak prominence as 0.15 of maximum signal in proestrous recording for each animal. Time taken between one trough to another in individual oscillations was calculated as the duration of each oscillation. The total duration of the surge signals was measured from their onset to offset. Onset was defined as the trough at the start of the first oscillation, and offset was defined as the trough at the end of the last oscillation.

To analyse the high frequency transients, the 30-minute moving average was subtracted from the original signal, and an additional exponential fit algorithm with a 400-second window was applied in MATLAB to correct baseline shifts. To identify significant calcium transients, the method of Dombeck and colleagues (Dombeck, Harvey et al. 2010) was adapted for GCaMP6s dynamics. First, the dF/F trace was z-scored such that its median was normalised to zero, and the standard deviation was set to one. Then, a series of thresholds iterated over the range 1 to 4 with step size 0.2: k = [1, 1.2, 1.4, …, 4] were defined. For each threshold k: positive and negative-going transients ($T_{pos}$ and $T_{neg}$) were identified. The z-scored trace was then thresholded such that z-score > k to generate a binary array. The segments of the array labelled as 1 (active transient) were classified as $T_{pos}$. The z-scored trace was also thresholded so that z-score < -k, producing another binary array, with segments labelled as 1 classified as $T_{neg}$. For each transient in $T_{pos}$, the transient significance was also assessed for its duration size s. The number of transients with sizes larger than s in both $T_{pos}$ and $T_{neg}$ were counted, as $n_{pos}$ and $n_{neg}$ respectively. If $n_{neg}/ n_{pos} < 0.05$, the positive transients with sizes greater than s were identified as significant. Any part of the trace identified as significant under any combination of k and s was considered a significant transient.

*Statistical Analysis*

All statistical analyses were performed using GraphPad Prism 10 software. Each dataset was tested for normality with Shapiro-Wilk test and visual inspection of Q-Q plots. Homogeneity of variance was tested by F-test when comparing two groups or Bartlett's test when comparing three or more groups. If data are normally distributed and variances are homogeneous, one-way

ANOVA, repeated measures one-way ANOVA with Geisser-Greenhouse correction followed by Tukey's multiple comparisons test, and paired t-tests were applied. Non-parametric tests, such as Friedman test followed by Dunn's multiple comparison tests were used when data are not normally distributed, or when the variances are not homogeneous. The threshold level for statistical significance was set at $p<0.05$.

**Acknowledgments**
This work was supported by the Wellcome Trust (212242/Z/18/Z) and a UKRI Medical Research Council Equipment Grant (MC-PC-MR-X012271/1). ZZ was supported by the UKRI Medical Research Council (MR N013433-1) and Harding Distinguished Postgraduate Scholars Programme Leverage Scheme. For the purpose of open access, the author has applied a Creative Commons Attribution (CC BY) license to any Author Accepted Manuscript version arising from this submission.

**Author Contributions:** ZZ undertook investigations; ZZ and CYH performed analysis; ZZ and AEH designed experiments and wrote the manuscript.

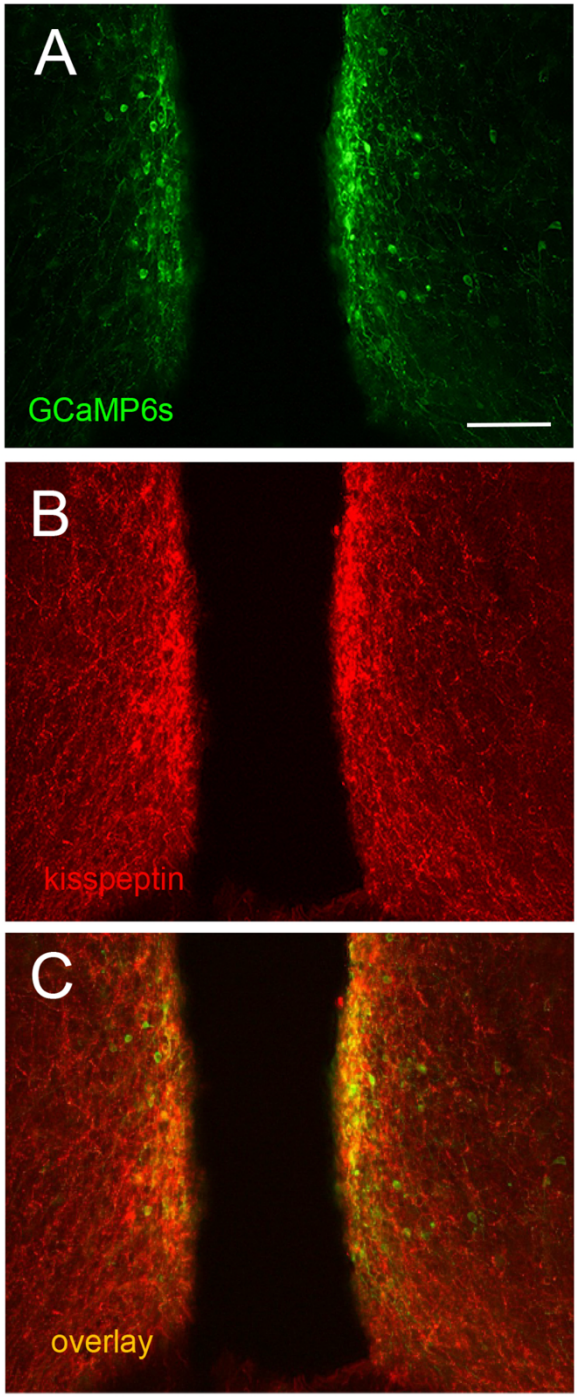


**Figure 1.** *GCaMP expression in RP3V$^{KISS}$ neurons*.
Confocal images of **(A)** GFP (GCaMP6s, green) and **(B)** kisspeptin (red) and immunofluorescence in the RP3V, and **(C)** an overlay of both in the periventricular nucleus of a proestrous female mouse. Scale bar = 100 µm.

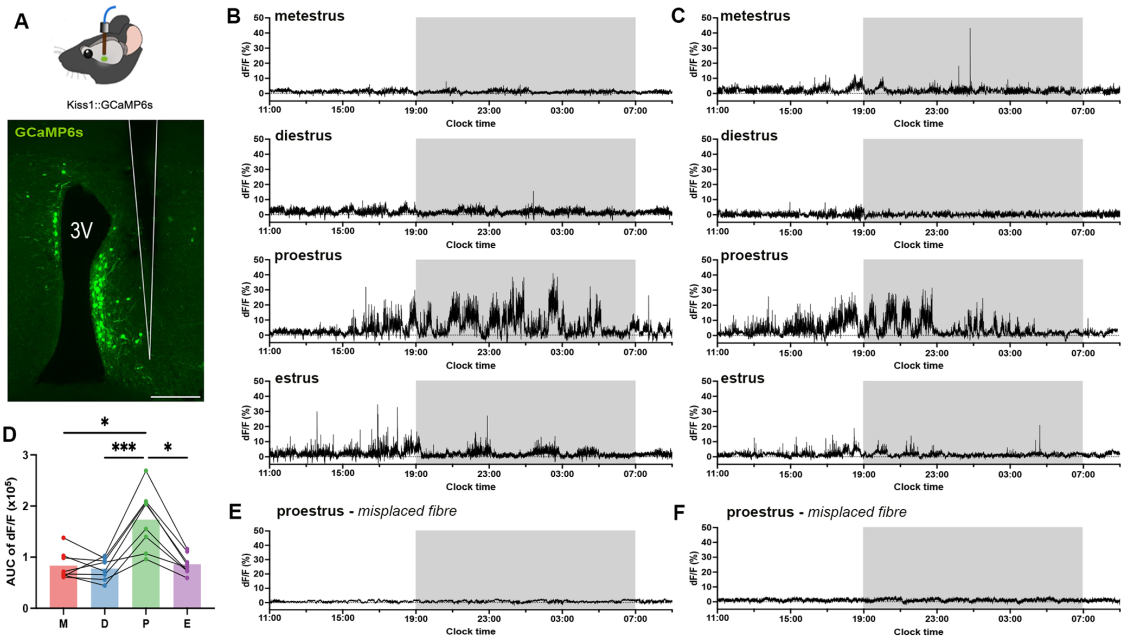


**Figure 2.** *GCaMP signals in RP3V$^{KISS}$ neurons across the estrous cycle.*
**(A)** Coronal section showing location of tapered optic fibre (white outline) in relation to GCaMP-expressing cells (green) lining the third ventricle (3V). Scale bar = 100 µm. **(B&C)** Two representative examples of 22-hour GCaMP fibre photometry recordings across the complete estrous cycle in two mice. Light-off period is represented by grey shaded area. **(D)** Mean area under the curve (AUC) calculated from 22-hour recordings across the estrous cycle: metestrus (M), diestrus (D), proestrus (P), and estrus (E). Each dot represents an animal (N=8). Friedman test followed by Dunn's multiple comparisons tests. * $p<0.05$, *** $p<0.001$. (**E&F**) Examples of 22-hour GCaMP fibre photometry recordings from two proestrous female mice with misplaced optic fibers in which signals remain < 3% of baseline.

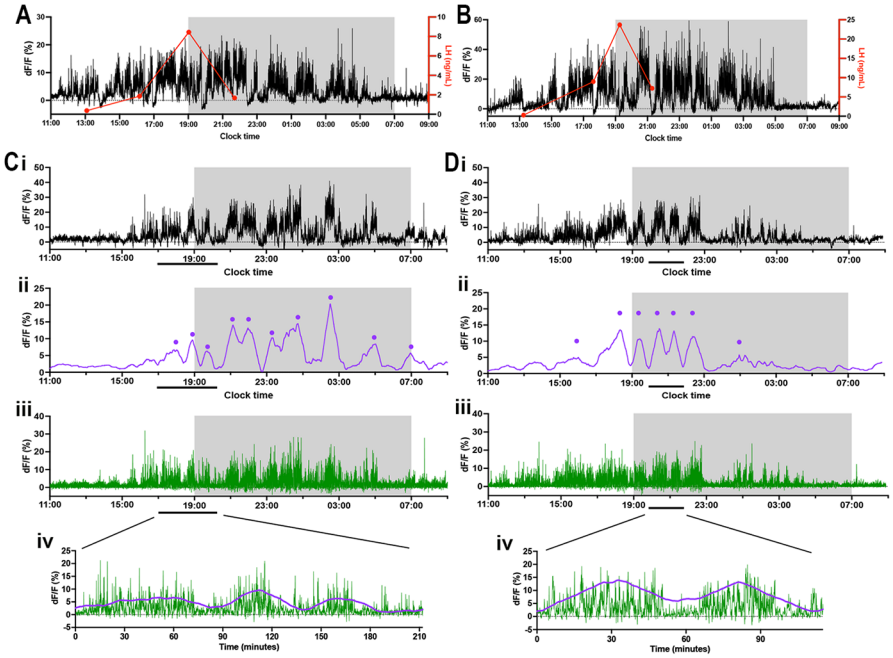


**Figure 3.** *Deconvolution of RP3V$^{KISS}$ neuron GCaMP signals and relation to the LH surge on proestrus.*

(**A,B**) Two representative examples showing the relationship between the increase in GCaMP activity (black) with luteinizing hormone (LH) surge (red). Light-off period is represented by grey shaded area. **(C,D)** Representative examples of 22-hour photometry recordings in proestrus from the same two female mice in Figure 2 showing (i) the original recording, (ii) a 30-minute moving average highlighting the baseline oscillations (purple) with identified oscillations labelled with dots, (iii) high frequency transients (green) after the moving average is subtracted from the original recording, (iv) expanded views of the traces showing moving average and high frequency transients. Light-off period is represented by grey shaded area.

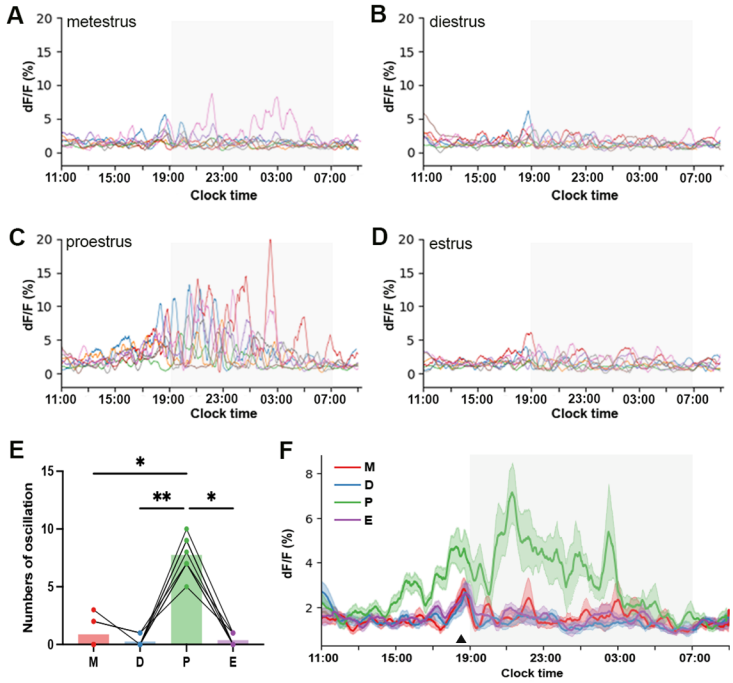


**Figure 4.** *Baseline oscillations of RP3V$^{KISS}$ neurons during proestrus.*
(**A-D**) Individual baseline oscillation traces from 22-hour recordings for each animal across each of the estrous cycle stages (n=8). (**E**) Mean number of oscillations identified across each stage of the estrous cycle. Each dot represents an animal (Friedman Test: $\chi^2$=18.75, p=0.0003; Dunn's multiple comparisons tests versus proestrus: p=0.0402 (metestrus), p=0.0029 (diestrus), p=0.0117 (estrus). (**F**) Mean baseline oscillations showing variations across the estrous cycle: metestrus (M, red), diestrus (D, blue), proestrus (P, green), and estrus (E, purple). Shaded regions around the traces indicate ± SEMs of corresponding colours (N=8). Triangle marks the oscillation occurring before lights-off. Light-off period is represented by grey shaded area.

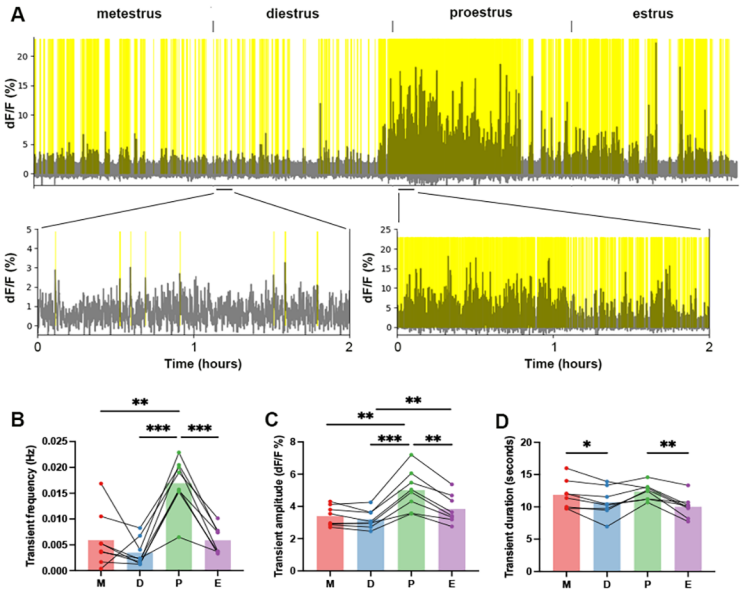


**Figure 5.** *Changes in RP3V$^{KISS}$ neuron high frequency transients across the cycle.*
(**A**) An example of high frequency transient signals across the estrous cycle in one mouse. Identified significant transients are highlighted in yellow and expanded views given below. Note different y-axes for diestrus and proestrous graphs. (**B**) Mean frequency (Hz), (**C**) amplitude (dF/F, %) and **(D)** duration (seconds) of transients in metestrus (M), diestrus (D), proestrus (P), and estrus (E). Each dot represents an animal (N=8). Repeated measures one-way ANOVA followed by Tukey's multiple comparisons test; * $p<0.05$, ** $p<0.01$, *** $p<0.001$ (see text for exact p values).

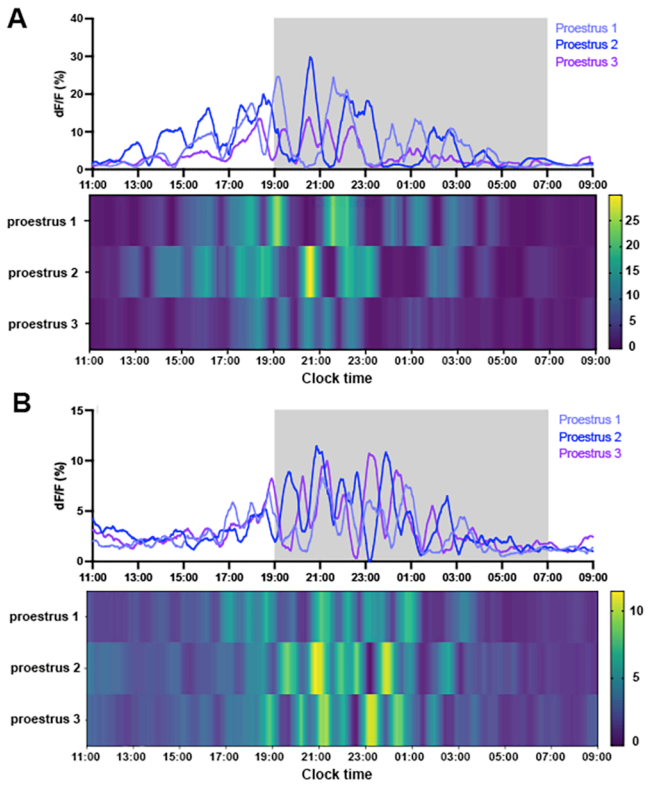


**Figure 6.** *Variable oscillations in RP3V$^{KISS}$ neuron activity across proestrous surges in the same mice.*

**(A&B)** Two representative examples showing code-extracted baseline profiles of RP3V$^{KISS}$ neuron GCaMP activity across three proestrous surges in the same mouse. Light-off period is represented by grey shaded area. Heat maps below show calcium signal dynamics (dF/F) with each row representing one proestrus. Colour intensity indicates dF/F values, with yellow and green colours representing higher signal amplitudes. Legends of heat maps show colour codes for dF/F (%).

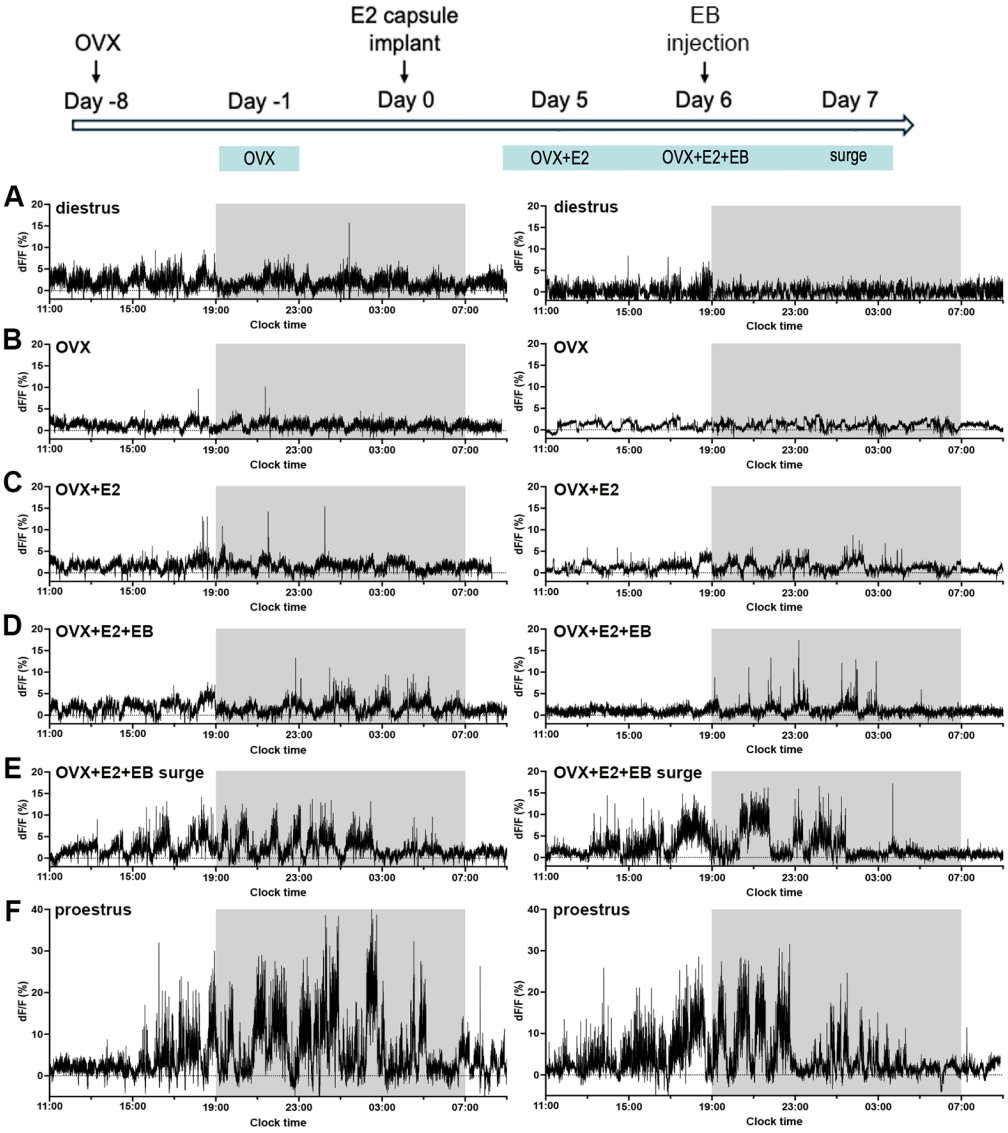


**Figure 7.** *Effects of ovariectomy and estrogen replacement on RP3V$^{KISS}$ neuron activity.* Experimental plan is shown at the top with times of photometry recordings highlighted in blue. Representative examples of 22-hour photometry recordings from two female mice (right and left) in **(A)** diestrus, (**B**) one week after OVX, (**C**) five days after the estradiol implant (OVX+E2), (**D**) on the day of estradiol benzoate injection (OVX+E2+EB), (**E**) at the time of the expected estradiol-induced LH surge (OVX+E2+EB surge), and for comparison (**F**) in proestrus (before ovariectomy). Light-off period is represented by grey shaded area.

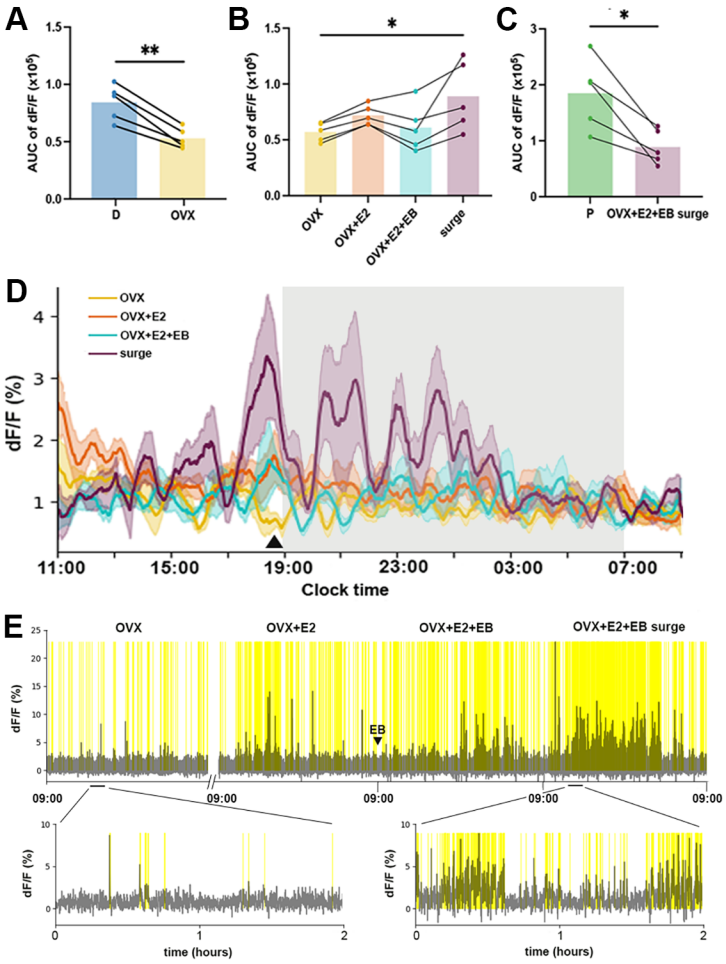


**Figure 8.** *Changing RP3V$^{KISS}$ neuron basal and transient activity following OVX + estrogen treatment regimens.*

(**A**) Mean area under the curve (AUC) of 22-hour recordings for mice in diestrus (D) and following their ovariectomy (OVX), paired t-test: p=0.002 (**B**) Mean AUC calculated in OVX, OVX+E2, OVX+E2+EB, and OVX+E2+EB surge conditions. Friedman test: $\chi^2$=10.68, p=0.0055, Dunn's multiple comparisons test p=0.021. (**C**) Mean AUC from intact proestrous mice (P) compared to the same mice under OVX+E2+EB surge conditions, paired t-test: p=0.014. Each dot represents one animal (N=5). (**D**) Mean moving average of baseline recordings over 22-hour recordings showing variations after OVX (yellow), five days after estradiol implant (OVX+E2, orange), on the day of EB injection (OVX+E2+EB, aqua), and on the day of OVX+E2+EB surge (plum). Shaded regions around the traces indicate SEMs of corresponding colours (n=5). Triangle marks the pre-lights-off oscillation. Light-off period is represented by grey shaded area. (**E**) Example of high frequency transient activity from a representative mouse 7 days after OVX and then continuously for three days encompassing the fifth day after E2 implant (OVX+E2), on the day of EB injection (OVX+E2+EB), and the day of the expected OVX+E2+EB LH surge. Triangle indicates time of EB injection. Identified significant transients are highlighted in yellow. Expanded views of the traces are shown below.

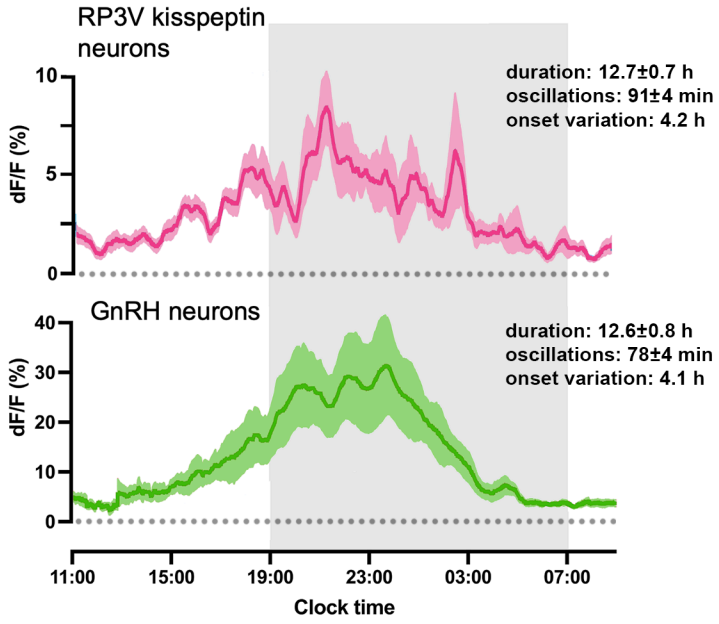


**Figure 9.** *Comparison between RP3V$^{KISS}$ and GnRH neuron activity patterns on proestrus.*

Mean 30-minute moving average of 22-hour GCaMP recordings across proestrus from RP3V$^{KISS}$ neurons (pink; taken from Fig.4F; N=8) and GnRH neuron dendron activity (green; raw data obtained from (Han, Yeo et al. 2025); n=7) processed in the same manner. Shaded regions around the traces indicate ± SEMs of corresponding colours. Text provides mean ± SEM duration of total elevated activity, duration of each oscillation, and variation in onset of oscillations between animals.

**References**

Bronson, F. H. (1981). "The regulation of luteinizing hormone secretion by estrogen: relationships among negative feedback, surge potential, and male stimulation in juvenile, peripubertal, and adult female mice." Endocrinology **108**(2): 506-516.
Bronson, F. H. and F. S. Vom Saal (1979). "Control of the preovulatory release of luteinizing hormone by steroids in the mouse." Endocrinology **104**(5): 1247-1255.
Clarkson, J., S. Y. Han, R. Piet, T. McLennan, G. M. Kane, J. Ng, R. W. Porteous, J. S. Kim, W. H. Colledge, K. J. Iremonger and A. E. Herbison (2017). "Definition of the hypothalamic GnRH pulse generator in mice." Proc Natl Acad Sci U S A **114**(47): E10216-E10223.
Clarkson, J., S. H. Yip, R. Porteous, A. Kauff, A. K. Heather and A. E. Herbison (2023). "CRISPR-Cas9 knockdown of ESR1 in preoptic GABA-kisspeptin neurons suppresses the preovulatory surge and estrous cycles in female mice." Elife **12**.
Coutinho, E. A., L. A. Esparza, P. H. Steffen, R. Liaw, S. Bolleddu and A. S. Kauffman (2024). "Selective depletion of kisspeptin neurons in the hypothalamic arcuate nucleus in early juvenile life reduces pubertal LH secretion and delays puberty onset in mice." FASEB J **38**(19): e70078.
Czieselsky, K., M. Prescott, R. Porteous, P. Campos, J. Clarkson, F. J. Steyn, R. E. Campbell and A. E. Herbison (2016). "Pulse and Surge Profiles of Luteinizing Hormone Secretion in the Mouse." Endocrinology **157**(12): 4794-4802.
Dombeck, D. A., C. D. Harvey, L. Tian, L. L. Looger and D. W. Tank (2010). "Functional imaging of hippocampal place cells at cellular resolution during virtual navigation." Nat Neurosci **13**(11): 1433-1440.
Dror, T., J. Franks and A. S. Kauffman (2013). "Analysis of multiple positive feedback paradigms demonstrates a complete absence of LH surges and GnRH activation in mice lacking kisspeptin signaling." Biol Reprod **88**(6): 146.
Glidewell-Kenney, C., L. A. Hurley, L. Pfaff, J. Weiss, J. E. Levine and J. L. Jameson (2007). "Nonclassical estrogen receptor alpha signaling mediates negative feedback in the female mouse reproductive axis." Proc Natl Acad Sci U S A **104**(19): 8173-8177.
Goodman, R. L., A. E. Herbison, M. N. Lehman and V. M. Navarro (2022). "Neuroendocrine control of gonadotropin-releasing hormone: Pulsatile and surge modes of secretion." J Neuroendocrinol **34**(5): e13094.
Goto, T., M. Hagihara, S. Irie, T. Abe, H. Kiyonari and K. Miyamichi (2025). "Dietary availability acutely influences puberty onset via a hypothalamic neural circuit." Neuron **113**(7): 1036-1050 e1035.
Goto, T., M. Hagihara and K. Miyamichi (2023). "Dynamics of pulsatile activities of arcuate kisspeptin neurons in aging female mice." Elife **12**.
Han, S. K., M. L. Gottsch, K. J. Lee, S. M. Popa, J. T. Smith, S. K. Jakawich, D. K. Clifton, R. A. Steiner and A. E. Herbison (2005). "Activation of gonadotropin-releasing hormone neurons by kisspeptin as a neuroendocrine switch for the onset of puberty." J Neurosci **25**(49): 11349-11356.
Han, S. Y., G. Kane, I. Cheong and A. E. Herbison (2019). "Characterization of GnRH Pulse Generator Activity in Male Mice Using GCaMP Fiber Photometry." Endocrinology **160**(3): 557-567.
Han, S. Y., P. G. Morris, J. C. Kim, S. Guru, M. Pardo-Navarro, S. H. Yeo, H. J. McQuillan and A. E. Herbison (2023). "Mechanism of kisspeptin neuron synchronization for pulsatile hormone secretion in male mice." Cell Rep **42**(1): 111914.

Han, S. Y., S. H. Yeo, J. C. Kim, Z. Zhou and A. E. Herbison (2025). "Multi-dimensional oscillatory activity of mouse GnRH neurons in vivo." Elife **13**.
Hellier, V., O. Brock, M. Candlish, E. Desroziers, M. Aoki, C. Mayer, R. Piet, A. Herbison, W. H. Colledge, V. Prevot, U. Boehm and J. Bakker (2018). "Female sexual behavior in mice is controlled by kisspeptin neurons." Nat Commun **9**(1): 400.
Herbison, A. E. (2008). "Estrogen positive feedback to gonadotropin-releasing hormone (GnRH) neurons in the rodent: the case for the rostral periventricular area of the third ventricle (RP3V)." Brain Res Rev **57**(2): 277-287.
Herbison, A. E. (2015). Physiology of the adult GnRH neuronal network. Knobil and Neill's Physiology of Reproduction. T. M. Plant and A. J. Zeleznik, Academic Press. **1:** 399-467.
Jamieson, B. B. and R. Piet (2022). "Kisspeptin neuron electrophysiology: Intrinsic properties, hormonal modulation, and regulation of homeostatic circuits." Front Neuroendocrinol **66**: 101006.
Karsch, F. J., J. M. Bowen, A. Caraty, N. P. Evans and S. M. Moenter (1997). "Gonadotropin-releasing hormone requirements for ovulation." Biol Reprod **56**: 303-309.
Kauffman, A. S. (2022). "Neuroendocrine mechanisms underlying estrogen positive feedback and the LH surge." Front Neurosci **16**: 953252.
Kreisman, M. J., R. B. McCosh and K. M. Breen (2022). "A Modified Ultra-Sensitive ELISA for Measurement of LH in Mice." Endocrinology **163**(9).
Liu, X., S. H. Yeo, H. J. McQuillan, M. K. Herde, S. Hessler, I. Cheong, R. Porteous and A. E. Herbison (2021). "Highly redundant neuropeptide volume co-transmission underlying episodic activation of the GnRH neuron dendron." Elife **10**.
Liu, Y., X. Shen, Y. Zeng, Y. Nie, J. Xu, A. E. Herbison, Y. Kuang and L. Wang (2025). "In-vivo properties and functional subtypes of gonadotropin-releasing hormone neurons." iScience **28**(5): 112513.
Matsuda, F., S. Ohkura, F. Magata, A. Munetomo, J. Chen, M. Sato, N. Inoue, Y. Uenoyama and H. Tsukamura (2019). "Role of kisspeptin neurons as a GnRH surge generator: Comparative aspects in rodents and non-rodent mammals." J Obstet Gynaecol Res **45**(12): 2318-2329.
McQuillan, H. J., J. Clarkson, A. Kauff, S. Y. Han, S. H. Yip, I. Cheong, R. Porteous, A. K. Heather and A. E. Herbison (2022). "Definition of the estrogen negative feedback pathway controlling the GnRH pulse generator in female mice." Nat Commun **13**(1): 7433.
McQuillan, H. J., S. Y. Han, I. Cheong and A. E. Herbison (2019). "GnRH Pulse Generator Activity Across the Estrous Cycle of Female Mice." Endocrinology **160**(6): 1480-1491.
Miller, B. H., S. L. Olson, F. W. Turek, J. E. Levine, T. H. Horton and J. S. Takahashi (2004). "Circadian clock mutation disrupts estrous cyclicity and maintenance of pregnancy." Curr Biol **14**(15): 1367-1373.
Minabe, S., Y. Uenoyama, H. Tsukamura and K. Maeda (2011). "Analysis of pulsatile and surge-like luteinizing hormone secretion with frequent blood sampling in female mice." J Reprod Dev **57**(5): 660-664.
Padilla, S. L., C. W. Johnson, F. D. Barker, M. A. Patterson and R. D. Palmiter (2018). "A Neural Circuit Underlying the Generation of Hot Flushes." Cell Rep **24**(2): 271-277.
Pau, K. F., M. Berria, D. L. Hess and H. G. Spies (1993). "Preovulatory gonadotropin-releasing hormone surge in ovarian-intact rhesus macaques." Endocrinology **133**: 1650-1656.
Piet, R. (2023). "Circadian and kisspeptin regulation of the preovulatory surge." Peptides **163**: 170981.

Piet, R., A. Fraissenon, U. Boehm and A. E. Herbison (2015). "Estrogen permits vasopressin signaling in preoptic kisspeptin neurons in the female mouse." J Neurosci **35**(17): 6881-6892.
Piet, R., B. Kalil, T. McLennan, R. Porteous, K. Czieselsky and A. E. Herbison (2018). "Dominant Neuropeptide Cotransmission in Kisspeptin-GABA Regulation of GnRH Neuron Firing Driving Ovulation." J Neurosci **38**(28): 6310-6322.
Pisano, F., M. Pisanello, S. J. Lee, J. Lee, E. Maglie, A. Balena, L. Sileo, B. Spagnolo, M. Bianco, M. Hyun, M. De Vittorio, B. L. Sabatini and F. Pisanello (2019). "Depth-resolved fiber photometry with a single tapered optical fiber implant." Nat Methods **16**(11): 1185-1192.
Porteous, R., P. Haden, E. C. R. Hackwell, A. Singline, M. K. Herde, R. Desai, D. J. Handelsman, D. R. Grattan and A. E. Herbison (2021). "Reformulation of PULSAR for Analysis of Pulsatile LH Secretion and a Revised Model of Estrogen-Negative Feedback in Mice." Endocrinology **162**(11).
Porteous, R. and A. E. Herbison (2019). "Genetic deletion of Esr1 in the mouse preoptic area disrupts the LH surge and estrous cyclicity." Endocrinology.
Sarkar, D. K., S. A. Chiappa, G. Fink and N. M. Sherwood (1976). "Gonadotropin-releasing hormone surge in pro-oestrous rats." Nature **264**: 461-463.
Silveira, M., L. L. Burger, R. A. DeFazio, E. R. Wagenmaker and S. M. Moenter (2017). "GnRH neuron activity and pituitary response in estradiol-induced vs proestrous luteinizing hormone surges in female mice." Endocrinology **158**: 356-366.
Skinner, D. C. and A. Caraty (2002). "Measurement and possible function of GnRH in cerebrospinal fluid in ewes." Reprod Suppl **59**: 25-39.
Starnes, A. N. and J. R. Jones (2023). "Inputs and Outputs of the Mammalian Circadian Clock." Biology (Basel) **12**(4).
Tonsfeldt, K. J., P. L. Mellon and H. M. Hoffmann (2022). "Circadian Rhythms in the Neuronal Network Timing the Luteinizing Hormone Surge." Endocrinology **163**(2).
Velasco, I., D. Franssen, S. Daza-Duenas, K. Skrapits, S. Takacs, E. Torres, E. Rodriguez-Vazquez, M. Ruiz-Cruz, S. Leon, K. Kukoricza, F. P. Zhang, S. Ruohonen, D. Luque-Cordoba, F. Priego-Capote, F. Gaytan, F. Ruiz-Pino, E. Hrabovszky, M. Poutanen, M. J. Vazquez and M. Tena-Sempere (2023). "Dissecting the KNDy hypothesis: KNDy neuron-derived kisspeptins are dispensable for puberty but essential for preserved female fertility and gonadotropin pulsatility." Metabolism **144**: 155556.
Wall, E. G., R. Desai, Z. K. Aung, S. H. Yeo, D. R. Grattan, D. J. Handelsman and A. E. Herbison (2023). "Unexpected plasma gonadal steroid and reproductive hormone levels across the mouse estrous cycle." BIORXIV-2023-530435v1-Herbison.
Wang, L., C. Vanacker, L. L. Burger, T. Barnes, Y. M. Shah, M. G. Myers and S. M. Moenter (2019). "Genetic dissection of the different roles of hypothalamic kisspeptin neurons in regulating female reproduction." Elife **8**.
Wintermantel, T. M., R. E. Campbell, R. Porteous, D. Bock, H. J. Grone, M. G. Todman, K. S. Korach, E. Greiner, C. A. Perez, G. Schutz and A. E. Herbison (2006). "Definition of estrogen receptor pathway critical for estrogen positive feedback to gonadotropin-releasing hormone neurons and fertility." Neuron **52**(2): 271-280.
Yeo, S. H., S. Y. Han and A. E. Herbison (2025). "Shifting GnRH Neuron Ensembles Underlie Successive Preovulatory Luteinizing Hormone Surges." J Neurosci **45**(3).
Yeo, S. H. and A. E. Herbison (2011). "Projections of arcuate nucleus and rostral periventricular kisspeptin neurons in the adult female mouse brain." Endocrinology **152**(6): 2387-2399.

Yeo, S. H., V. Kyle, P. G. Morris, S. Jackman, L. C. Sinnett-Smith, M. Schacker, C. Chen and W. H. Colledge (2016). "Visualisation of Kiss1 neurone distribution using a Kiss1-CRE transgenic mouse." J Neuroendocrinol **28**(11).
Yip, S. H., U. Boehm, A. E. Herbison and R. E. Campbell (2015). "Conditional viral tract tracing delineates the projections of the distinct kisspeptin neuron populations to GnRH neurons in the mouse." Endocrinology **156**(7): 2582-2594.
Zhou, Z., S. Y. Han, M. Pardo-Navarro, E. G. Wall, R. Desai, S. Vas, D. J. Handelsman and A. E. Herbison (2025). "GnRH pulse generator activity in mouse models of polycystic ovary syndrome." Elife **13**.